Check for updates

Metal-free porous phosphorus-doped g-C₃N₄ photocatalyst achieving efficient synthesis of benzoin†

Yuanjin Li,‡[a] Shuhui Wang,‡*[a] Jin Wu,[b] Qiuyan Wang, [ID][a] Changqiu Ma,[a] Daheng Jiang,[a] Wanglai Hu,*[c] Lixin Zhu*[b] and Xiaoliang Xu [ID] *[a]

Photocatalytic organic synthesis is mostly limited by the shortcomings of insufficient light absorption, high photogenerated electron–hole recombination rate and inadequate reactive sites of photocatalysts. To solve these problems, phosphorus-doped g-C₃N₄ with a porous structure was constructed. Benefiting from enhanced light absorption and electron–hole separation efficiency, PCNT has intensive oxygen activation ability to generate superoxide radicals, and is highly active in organic synthesis. In addition, PCNT has enhanced surface nucleophilicity, which is conducive to the carbon–carbon coupling process of the intermediate product benzaldehyde molecules and benzyl alcohol molecules in the benzoin condensation reaction. Metal-free PCNT is expected to replace the previously used highly toxic cyanide catalysts and provide a new way for the low-cost and efficient photocatalytic synthesis of benzoin.

1. Introduction

Organic synthetic chemistry has constructed a rich and colourful world and plays an increasingly important role in people's life.[1,2] The pursuit of green and efficient synthetic methods has always been the development direction of organic synthesis chemistry. Among them, photocatalytic organic synthesis has become a potential organic synthesis method due to its advantages of utilizing renewable solar energy and mild reaction conditions.[3–6] Benzoin, as an important organic synthesis intermediate, has wide applications in the production of medicines, spices and daily chemicals.[7–9] However, the current catalytic oxidation synthesis of benzoin usually uses highly toxic cyanide as a catalyst, which is likely to cause pollution during the operation, significantly limiting its further applications.[10] Therefore, there is an urgent need to design and construct a cheap and environmentally friendly heterogeneous photocatalyst for efficient benzoin condensation reaction.

Graphite carbon nitride (g-C₃N₄) is a polymer semiconductor material with a layered structure similar to graphite, in which carbon and nitrogen atoms are tightly combined into rings by covalent bonds, which has the advantages of simple and convenient synthesis, low toxicity and high chemical stability.[11–14] Because of its proper electronic energy band position and outstanding physical and chemical properties, g-C₃N₄ is considered as a developing photocatalyst, which has been used in various photocatalytic applications, such as water splitting,[15–18] CO_2 reduction,[11,19,20] pollutant degradation,[21–23] and organic synthesis.[24–27] Generally, an effective photocatalyst needs to have strong and broad light absorption, effective photogenerated carrier separation efficiency, appropriate energy band position, and enough reactive sites to make active substances (such as electrons and reactive oxygen species) participate in the catalytic process. Therefore, these properties can determine the efficiency of photocatalytic organic synthesis. For improvement of relevant catalysts, porous structure and element doping are two crucial methods.[11,28–30] Among them, the porous structure helps the catalyst expose more active sites, and the reactants and products are more easily to diffuse in the catalyst, thereby helping to accelerate the reaction process. Element doping can change the electronic state density of the catalyst, facilitate the separation and redistribution of charges in the catalyst, and can provide more charge for the photocatalytic reaction and improve the photocatalytic performance.

Herein, we synthesized porous phosphorus-doped g-C₃N₄ (PCNT) through the combination of mixed precursors and thermal exfoliation. PCNT has excellent photocatalytic performance and can be used in the selective oxidative coupling reaction of benzyl alcohol. A detailed study of the reaction process shows that the synthesis of benzoin from benzyl alcohol is divided into two steps, in which benzaldehyde is an intermediate product in the reaction process, and the enhanced

[a]School of Physical Sciences, University of Science and Technology of China, Hefei, Anhui 230026, PR China. E-mail: wsh2016@mail.ustc.edu.cn; xlxu@ustc.edu.cn

[b]Department of General Surgery & Central Laboratory, The First Affiliated Hospital of Anhui Medical University, Hefei, Anhui 230022, PR China. E-mail: lx-zhu@163.com

[c]Translational Research Institute of Henan Provincial People's Hospital, Molecular Pathology Center of Academy of Medical Science, Zhengzhou University, Zhengzhou, Henan 450003, PR China. E-mail: wanglaihu@ahmu.edu.cn

‡ These authors contributed equally to this work.

nucleophilicity of PCNT is beneficial to the occurrence of the carbon–carbon coupling process. This is the first report of using a completely non-metallic photocatalyst in the condensation of benzoin. As a photocatalyst, PCNT can reduce production costs and increase the conversion rate of reaction raw materials, and the catalyst can be easily recycled as well. It is a new way to efficiently synthesize benzoin and conform to the new concept of modern green chemistry.

2. Experimental

2.1 Synthesis of photocatalysts

All reagents are analytical grade chemicals, directly used without further depuration. Phosphorus-doped g-C_3N_4 (PCN) was synthesized by thermal condensation of mixed precursors (2-aminoethylphosphonic acid and melamine). More concretely, 6 g of melamine (ME) and 100 mg of 2-amino-ethylphosphonic acid (AEP) were uniformly mixed and placed in a covered quartz boat (the optimal doping concentration was determined by preliminary research in Fig. S1†). The mixture was heated to 550 °C from 30 °C within 52 minutes, maintained for 6 h, then naturally cooled. The obtained PCN was treated with thermal exfoliation to synthesize porous PCNT. In detail, the PCN was heated in an open crucible to 500 °C, kept for 90 minutes, then cooled naturally. The product was ground into powder to obtain PCNT. In the same way without AEP, ordinary g-C_3N_4 (CN) and thermally peeled g-C_3N_4 (CNT) were prepared.

2.2 Nitroblue tetrazole (NBT) degradation experiments

50 mg of photocatalyst was mixed with 50 mL NBT solution (200 mM), illuminated by a 300 W xenon lamp (PLS-SXE300/300UV, Trusttech Co., Ltd., Beijing). The concentration of NBT was monitored by UV-visible spectra (Perkin Elmer Lambda950) every 30 minutes, as the absorption peak of NBT is located at 259 nm.

2.3 Electron spin resonance (ESR) tests

500 μL of 5,5-dimethyl-1-pyrrolidine-N-oxide (DMPO, 10 mM) was added into 50 μL sample aqueous solution (10 g L^{-1}). After being irradiated for 1 min with a xenon lamp (same as above), the mixed solution was characterized using a JEOL JES-FA200 electron spin resonance spectrometer (298 K, 9.062 GHz).

2.4 Photocatalytic synthesis of benzoin

10 mg of photocatalyst and 2 mL of benzotrifluoride were mixed in a 10 mL quartz tube. After sonication, 0.1 mmol of benzyl alcohol was added and oxygen was bubbled for one minute. Then the quartz tube was sealed and irradiated with a xenon lamp (the same as that in ESR tests) for 6 h. The photocatalyst was removed by centrifugation, and the reaction solution was collected. The product was measured by a 400 MHz 1H Bruker AVANCE AV III NMR spectrometer, using tetramethylsilane as an internal standard. Conversion rate is the ratio of reduced benzyl alcohol concentration to initial benzyl alcohol concentration. The yield rate is the proportion of benzyl alcohol concentration consumed by the target product in the initial benzyl alcohol concentration. Selectivity is the ratio of yield rate to conversion rate.

3. Results and discussion

In this work, PCNT was prepared by phosphorus doping and thermal exfoliation. The characteristic crystal structures of all prepared samples are shown in Fig. 1a, the two crystal planes of (100) and (002) are corresponding to the standard patterns (JCPDS 87-1526), indicating high purity of all samples. Compared with CN, the (002) diffraction peak of PCN obviously moves to a lower angle due to the introduction of phosphorus element with a larger atomic radius, and the peak moves back slightly after thermal exfoliation. Energy Dispersive Spectrometer confirms the equidistribution of P, C and N elements in PCNT (Fig. 1b). The chemical structure and composition of PCNT were further studied by X-ray photoelectron spectroscopy (XPS) and X-ray absorption near edge structure (XANES). Compared with that of CNT, the N 1s spectrum of PCNT shifts to the direction of higher binding energy (Fig. 1c), and the peak located at 133.8 eV binding energy in the P 2p spectrum of PCNT can be attributed to the P–N bond (Fig. S2†).[31,32] Therefore, it can be inferred that P replaces C in the structural unit of g-C_3N_4. As shown by the N K-edge spectra of Fig. 1d, the peak belonging to C–N–C is obviously shifted, which further supports the above conclusion.

On the other hand, the AEP added in the synthesis process of PCN and PCNT can not only be used as a phosphorus source, but also can be used as a gas phase template for sample growth. AEP can generate ammonia during the heating process, which will create a porous structure in the sample.[33] A further thermal peeling process can reduce the thickness of the sample and expose these holes. The porous structure of PCNT was ocularly characterized by the transmission electron microscopy (TEM) and scanning electron microscopy images in Fig. 2a and S3.† In contrast, CN has a thick and large aggregate morphology
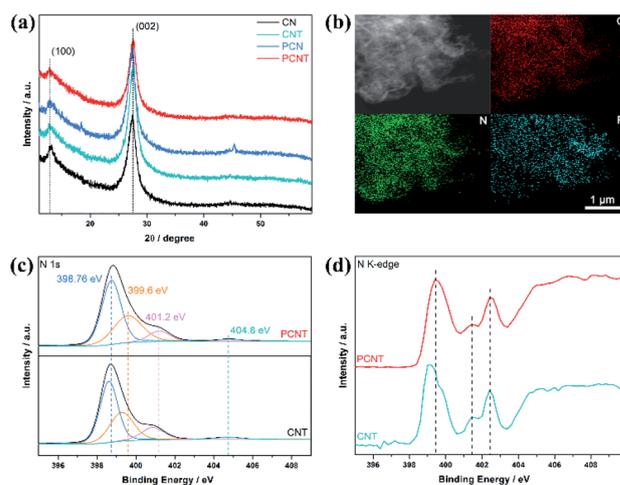

Fig. 1 (a) X-ray diffraction results of CN, CNT, PCN, and PCNT. (b) Elemental mapping images of PCNT. (c) XPS N 1s spectra of PCNT and CNT. (d) XANES N K-edge spectra of PCNT and CNT.
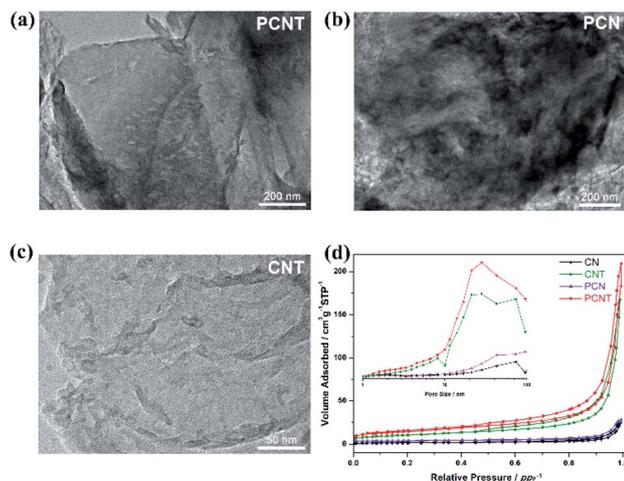
Fig. 2 (a–c) TEM images of (a) PCNT, (b) PCN, and (c) CNT. (d) Nitrogen adsorption–desorption isotherms of CN, CNT, PCN, and PCNT with the inset displaying the corresponding pore size distribution curves.

Fig. 3 (a) UV-vis absorption spectra, (b) corresponding band gap, (c) schematic illustration of band structure, and (d) photoluminescence spectra of CN, CNT, PCN, and PCNT.

(Fig. S3†), PCN has a rough undulating surface (Fig. 2b), while CNT has a non-porous sheet structure (Fig. 2c and S4†). The BET surface area of all samples was compared by nitrogen adsorption–desorption curve. As displayed in Fig. 2d, both samples show IV type isotherms, indicating the presence of mesopores in the samples.[34] Under higher relative pressure, the isotherms of PCNT show higher absorption rates, indicating that there are large mesopores and macropores. The unique porous structure of PCNT results in a relatively large specific surface area, which exposes more active sites. At the same time, the presence of pores facilitates the diffusion of reactants and products molecules in the photocatalytic process, which is beneficial to the improvement of catalytic activity.

As the first step of the photocatalytic reaction process, only when photocatalysts absorb sufficient light energy, can photogenerated electron–hole pairs be produced in photocatalysts. In this case, light absorption efficiency much affects the photocatalytic reaction efficiency.[35] UV-visible diffuse reflectance spectroscopy was conducted to study the optical properties and band structure of the prepared samples. As displayed in Fig. 3a, phosphorus doping makes the light absorption of PCN and PCNT significantly increase over a large range. The porous structure caused by phosphorus doping increases the reflection of light in the holes, which may lead to enhanced light absorption. Meanwhile, the absorption edge of PCN and PCNT extend to the high wavelength direction. Due to the quantum confinement effect, the light absorption of the two thermally stripped samples is slightly blue-shifted compared with that of original samples.[36,37] The typical light absorption edges of CN, CNT, PCN, and PCNT are located at approximately 454, 444, 471 and 468 nm, corresponding to the indirect band gaps of 2.73, 2.79, 2.63 and 2.65 eV, respectively (Fig. 3b). Combined with the XPS valence band spectra (Fig. S5†), the band structures of several samples are schematically shown in Fig. 3c. Furthermore, the separation efficiency of photogenerated carriers of all
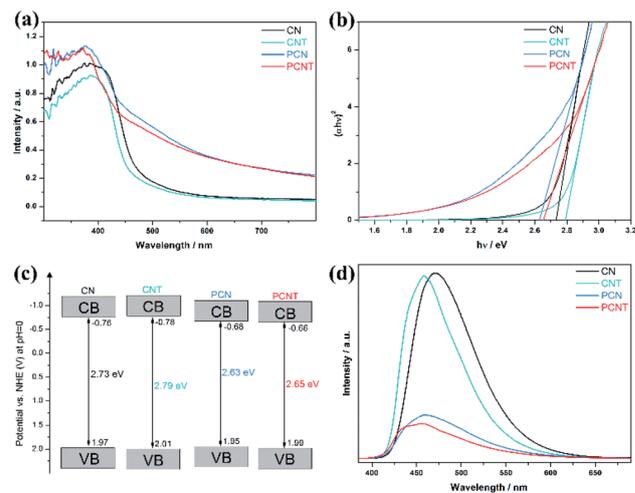
photocatalysts was detected through photoluminescence spectra. As displayed in Fig. 3d, CN has the relatively strongest photoluminescence intensity, indicating the serious recombination of the photogenerated electrons and holes in it. For CNT and PCNT, their photoluminescence position has a significant blue shift relative to the corresponding bulk materials, which is consistent with the UV-visible absorption spectroscopy. PCN and PCNT have significantly reduced luminous intensity, proving that phosphorous doping can effectively hinder the recombination of photogenerated carriers. For PCNT, enhanced light absorption is conducive to utilizing more solar energy and generating more photogenerated carriers, and the effective separation of photogenerated carriers ensures that there are enough electrons and holes for photocatalytic reactions.
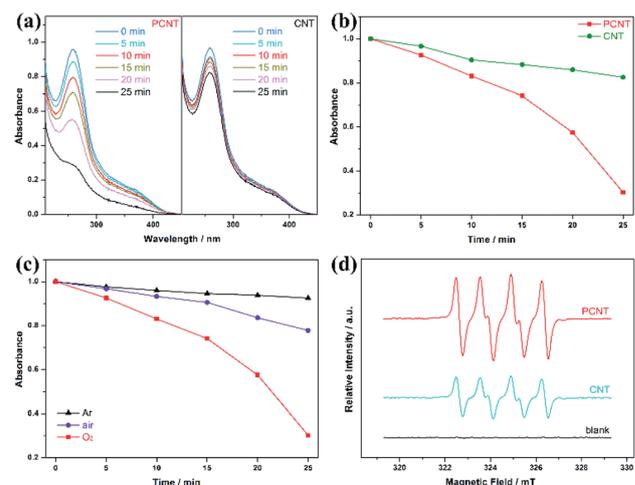

Fig. 4 (a) The degradation process of NBT with PCNT and CNT in O_2. (b) Time-dependent NBT concentration curve in the degradation process. (c) Time-dependent NBT degradation process with PCNT in gas conditions. (d) ESR spectra of PCNT and CNT after adding DMPO.

Phosphorus doping is favourable in oxygen activation, which is proved with nitroblue tetrazole (NBT) as a probe molecule for generated $O_2^{\bullet-}$ radicals.[38] As displayed in Fig. 4a and b, the time-dependent absorption spectra of NBT degradation in oxygen displays the enhanced oxygen activation ability of PCNT. Besides, the dramatically different NBT degradation rates decreased significantly under the condition of oxygen-deficiency (air) and oxygen-free (argon), indicating that the $O_2^{\bullet-}$ evolve from oxygen (Fig. 4c). Electron spin resonance (ESR) tests can also evaluate the presence of $O_2^{\bullet-}$. When DMPO was used as a scavenger to detect the $O_2^{\bullet-}$ formation in the system, significantly enhanced sextet ESR signals of DMPO-$O_2^{\bullet-}$ adducts were clearly observed in both PCNT and CNT, confirming the generation of $O_2^{\bullet-}$ (Fig. 4d). Moreover, the DMPO-$O_2^{\bullet-}$ signal of PCNT is obviously stronger than that of CNT, suggesting the enhanced $O_2^{\bullet-}$ generation ability, which is well in agreement with the above oxygen activation tests.

The synthesis of benzoin with benzyl alcohol further confirmed the excellent photocatalytic performance of PCNT. As shown in Fig. 5a, after 6 hours of xenon lamp irradiation, the conversion rate of benzyl alcohol can reach 99.8% with PCNT as the photocatalyst, and the yield of benzoin can reach 95.4% with fairly high selectivity. For CN, CNT and PCN, they can only catalyse the oxidation of benzyl alcohol to a small amount of benzaldehyde (Fig. S6†). The reaction time was further extended to 12 hours, and there was still no benzoin formation on CN, CNT, and PCN. Moreover, prolonging the reaction time has almost no effect on the amount of benzaldehyde produced on these catalysts. In addition, the cyclic stability of PCNT in the photocatalytic benzyl synthesis process was further studied. After 5 consecutive cycles, the conversion rate of benzyl alcohol and the yield of benzoin remained basically unchanged, indicating that PCNT has good cycle stability.

In the benzoin synthesis process with PCNT as a photocatalyst, no by-products were detected except for benzaldehyde,

so it is speculated that benzaldehyde is an intermediate product in the synthesis process of benzoin from benzyl alcohol. To verify this, we monitored the changes in the content of benzaldehyde and benzoin over time. As shown in Fig. 5b and c, only benzaldehyde was produced at the beginning. After 3 hours of light irradiation, the yield of benzaldehyde reached the highest value of 41.8%. As the reaction continues, the content of benzaldehyde begins to decrease, and benzoin is gradually formed, eventually reaching a high benzoin yield. According to this trend, we confirmed the accumulation and consumption of benzaldehyde in the reaction process, and benzaldehyde is an intermediate product of the reaction. One of the reasons why CN, CNT and PCN cannot catalyze the formation of benzoin is that sufficient concentration of benzaldehyde is not produced during the reaction. In addition, we used benzaldehyde as the raw material for the photocatalytic synthesis of benzoin, and only the conversion rate and selectivity of benzaldehyde to benzoin on PCNs both reached 99%.

Based on the above experimental results, we analyzed the reaction mechanism, which is schematically shown in Fig. 5d. In the synthesis process of benzoin from benzyl alcohol, the formation of benzaldehyde is the first step, and $O_2^{\bullet-}$ is the key reactive oxygen species for the formation of benzaldehyde. Benefiting from the enhanced ability to generate superoxide radicals, PCNT can more effectively photocatalyze the selective photo-oxidation of benzyl alcohol to benzaldehyde. When the concentration of benzaldehyde in the reaction system is sufficient, the C–C coupling of benzaldehyde molecules occurs in the synthesis process of benzoin.[39] In the C–C coupling process, polarity of the photocatalyst is of critical importance. As shown by the zeta potential results (Fig. S7†), compared with the original CN, the zeta potential of PCNT is doubled, and the potential of PCNT is the lowest among all the catalysts, which proves that the surface of PCNT has more negative charges. PCNT is a catalyst with more nucleophilic surface properties,[40] so it is easier to connect to the carbon ions in the benzaldehyde carbonyl group, and drive the C–C coupling process of benzaldehyde. Finally, the efficient conversion from benzyl alcohol to benzoin is achieved on PCNT.

4. Conclusions

In summary, the problem of insufficient light absorption and serious recombination of photogenerated carriers of g-C_3N_4 is solved by the strategy of phosphorus doping, resulting in enhanced photocatalytic activity. Using mixed precursor thermal condensation and subsequent thermal peeling methods, we prepared phosphorus-doped PCNT with a porous structure. The introduction of P element was demonstrated by different characterizations. The porous structure of PCNT was verified by TEM image, SEM image and nitrogen adsorption–desorption curve. PCNT achieved enhanced light absorption capacity and effective photogenerated carriers separation, and have enhanced oxygen activation capacity. As a result, the photocatalytic synthesis process of benzoin from benzyl alcohol can be efficiently realized on PCNT, with benzaldehyde as the intermediate product in the reaction. PCNT is easy to prepare,
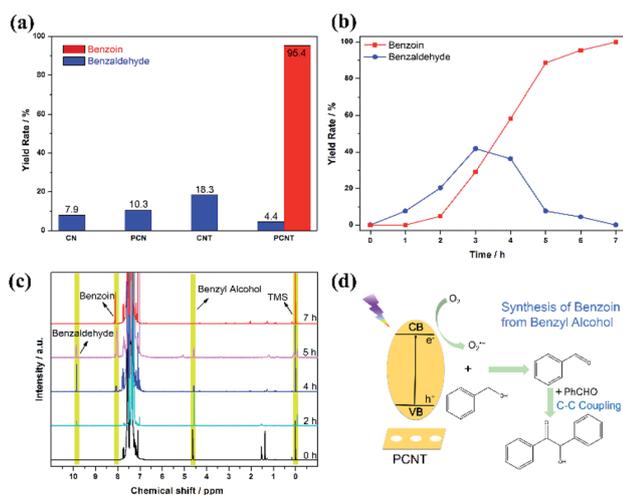

Fig. 5 (a) Yield rate of benzoin and benzaldehyde on different photocatalysts within 6 h. (b) Time-dependent yield rate of benzoin and benzaldehyde with PCNT as photocatalyst. (c) Representative ^{1}H NMR spectra of photocatalytic reaction process on PCNT at different times. (d) Schematic synthesis mechanism of benzoin from benzyl alcohol.

do not contain any metal elements, and is an environmentally friendly photocatalyst. This work is expected to apply cheap, non-polluted and metal-free semiconductor materials for achieving effective photocatalytic organic synthesis reactions under environmental conditions.

Conflicts of interest

There are no conflicts to declare.

Acknowledgements

References

1 J. Xiao, X. Liu, L. Pan, C. Shi, X. Zhang and J. Zou, *ACS Catal.*, 2020, **10**, 12256.

2 D. Franchi and Z. Amara, *ACS Sustainable Chem. Eng.*, 2020, **8**, 15405.

3 F. Parrino, M. Bellardita, E. I. García-López, G. Marcì, V. Loddo and L. Palmisano, *ACS Catal.*, 2018, **8**, 11191.

4 S. Zhang, Y. Zhao, R. Shi, C. Zhou, G. I. N. Waterhouse, L. Wu, C. H. Tung and T. Zhang, *Adv. Energy Mater.*, 2020, **10**, 1901973.

5 Y. Zhao, Y. Zhao, R. Shi, B. Wang, G. I. N. Waterhouse, L. Z. Wu, C. H. Tung and T. Zhang, *Adv. Mater.*, 2019, **31**, 1806482.

6 X. Sun, X. Luo, X. Zhang, J. Xie, S. Jin, H. Wang, X. Zheng, X. Wu and Y. Xie, *J. Am. Chem. Soc.*, 2019, **141**, 3797.

7 E. Frick, C. Schweigert, B. B. Noble, H. A. Ernst, A. Lauer, Y. Liang, D. Voll, M. L. Coote, A. N. Unterreiner and C. Barner-Kowollik, *Macromolecules*, 2016, **49**, 80.

8 P. Burger, A. Casale, A. Kerdudo, T. Michel, R. Laville, F. Chagnaud and X. Fernandez, *Food Chem.*, 2016, **210**, 613.

9 J. Du, H. Singh and T. H. Yi, *Bioprocess Biosyst. Eng.*, 2016, **39**, 1923.

10 Y. He and Y. Xue, *J. Phys. Chem. A*, 2010, **114**, 9222.

11 S. Wang, J. Zhan, K. Chen, A. Ali, L. Zeng, H. Zhao, W. Hu, L. Zhu and X. Xu, *ACS Sustainable Chem. Eng.*, 2020, **8**, 8214.

12 Y. Li, S. Jin, X. Xu, H. Wang and X. Zhang, *J. Appl. Phys.*, 2020, **127**, 170903.

13 H. Wang, S. Jiang, W. Liu, X. Zhang, Q. Zhang, Y. Luo and Y. Xie, *Angew. Chem., Int. Ed.*, 2020, **59**, 11093.

14 F. He, Z. Wang, Y. Li, S. Peng and B. Liu, *Appl. Catal., B*, 2020, **269**, 118828.

15 Y.-P. Zhu, T. –Z. Ren and Z. –Y. Yuan, *ACS Appl. Mater. Interfaces*, 2015, **7**, 16850.

16 M. Zhu, S. Kim, L. Mao, M. Fujitsuka, J. Zhang, X. Wang and T. Majima, *J. Am. Chem. Soc.*, 2017, **139**, 13234.

17 X. Wang, K. Maeda, A. Thomas, K. Takanabe, G. Xin, J. M. Carlsson, K. Domen and M. Antonietti, *Nat. Mater.*, 2009, **8**, 76.

18 J. Liu, Y. Liu, N. Liu, Y. Han, X. Zhang, H. Huang, Y. Lifshitz, S. T. Lee, J. Zhong and Z. Kang, *Science*, 2015, **347**, 970.

19 A. Li, T. Wang, C. Li, Z. Huang, Z. Luo and J. Gong, *Angew. Chem., Int. Ed.*, 2019, **58**, 3804.

20 K. Wang, Q. Li, B. Liu, B. Cheng, W. Ho and J. Yu, *Appl. Catal., B*, 2015, **176**, 44.

21 M. Chu, K. Hu, J. Wang, Y. Liu, S. Ali, C. Qin and L. Jing, *Appl. Catal., B*, 2019, **243**, 57.

22 T. Xiong, W. Cen, Y. Zhang and F. Dong, *ACS Catal.*, 2016, **6**, 2462.

23 M. Zhang, X. Bai, D. Liu, J. Wang and Y. Zhu, *Appl. Catal., B*, 2015, **164**, 77.

24 X. Sun, D. Jiang, L. Zhang and W. Wang, *Appl. Catal., B*, 2018, **220**, 553.

25 F. Su, S. C. Mathew, L. Möhlmann, M. Antonietti, X. Wang and S. Blechert, *Angew. Chem., Int. Ed.*, 2011, **50**, 657.

26 H. Wang, X. Sun, D. Li, X. Zhang, S. Chen, W. Shao, Y. Tian and Y. Xie, *J. Am. Chem. Soc.*, 2017, **139**, 2468.

27 H. Wang, S. Jiang, S. Chen, D. Li, X. Zhang, W. Shao, X. Sun, J. Xie, Z. Zhao, Q. Zhang, Y. Tian and Y. Xie, *Adv. Mater.*, 2016, **28**, 6940.

28 J. Ran, T. Y. Ma, G. Gao, X. W. Du and S. Z. Qiao, *Energy Environ. Sci.*, 2015, **8**, 3708.

29 S. Hu, L. Ma, J. You, F. Li, Z. Fan, F. Wang, D. Liu and J. Gui, *RSC Adv.*, 2014, **4**, 21657.

30 A. Dandia, S. L. Gupta, P. Saini, R. Sharma, S. Meena and V. Parewa, *Curr. Res. Green Sustainable Chem.*, 2020, **3**, 100039.

31 Y. Zhang, T. Mori, J. Ye and M. Antonietti, *J. Am. Chem. Soc.*, 2010, **132**, 6294.

32 S. Guo, Z. Deng, M. Li, B. Jiang, C. Tian, Q. Pan and H. Fu, *Angew. Chem., Int. Ed.*, 2016, **55**, 1830.

33 M. Zhang, J. Xu, R. Zong and Y. Zhu, *Appl. Catal., B*, 2014, **147**, 229.

34 X. Zhou, Z. Luo, P. Tao, B. Jin, Z. Wu and Y. Wang, *Mater. Chem. Phys.*, 2014, **143**, 1462.

35 G. Liu, P. Niu, C. Sun, S. C. Smith, Z. Chen, G. Q. Lu and H. M. Cheng, *J. Am. Chem. Soc.*, 2010, **132**, 11642.

36 H. Xu, J. Yan, X. She, L. Xu, J. Xia, Y. Xu, Y. Song, L. Huang and H. Li, *Nanoscale*, 2014, **6**, 1406.

37 Q. Lin, L. Li, S. Liang, M. Liu, J. Bi and L. Wu, *Appl. Catal., B*, 2015, **163**, 135.

38 J. Huang, L. Dou, J. Li, J. Zhong, M. Li and T. Wang, *J. Hazard. Mater.*, 2021, **403**, 123857.

39 J. E. Perez, M. Kumar, J. S. Francisco and A. Sinha, *J. Phys. Chem. A*, 2017, **121**, 1022.

40 K. Ranjan, K. Dharamvir and V. K. Jindal, *Phys. B*, 2005, **365**, 121.